The Astrophysical Journal, 965:114 (10pp), 2024 April 20 https://doi.org/10.3847/1538-4357/ad2fab

Prediction for Arrival Time and Parameters of Corotation Interaction Regions using Earth–Mars Correlated Events from Tianwen-1, MAVEN, and Wind Observations

Zhihui Zhong[1], Chenglong Shen[1,2], Yutian Chi[3], Dongwei Mao[4], Bin Miao[5], Zhiyi Fu[4], Junyan Liu[4], Beatriz Sánchez-Cano[6], Daniel Heyner[7], and Yuming Wang[1,2,8]
[1] Deep Space Exploration Laboratory/School of Earth and Space Sciences, University of Science and Technology of China, Hefei, 230026, People's Republic of China; clshen@ustc.edu.cn
[2] CAS Center for Excellence in Comparative Planetology, University of Science and Technology of China, Hefei, 230026, People's Republic of China
[3] Institute of Deep Space Sciences, Deep Space Exploration Laboratory, Hefei, 230026, People's Republic of China; ytchi@mail.ustc.edu.cn
[4] CAS Key Laboratory of Geospace Environment, Department of Geophysics and Planetary Sciences, University of Science and Technology of China, Hefei, 230026, People's Republic of China
[5] Institute of Advanced Technology, University of Science and Technology of China, Hefei, 230026, People's Republic of China
[6] School of Physics and Astronomy, University of Leicester, Leicester, UK
[7] Institut für Geophysik und extraterrestrische Physik, Technische Universität Braunschweig, Braunschweig, Germany
[8] Anhui Mengcheng Geophysics National Observation and Research Station, University of Science and Technology of China, Mengcheng, Anhui, People's Republic of China
Received 2024 February 3; revised 2024 February 26; accepted 2024 March 1; published 2024 April 12

Abstract

Using the Stream Interaction Regions list from the Tianwen-1/Mars Orbiter Magnetometer (MOMAG) data between 2021 November and 2021 December and from Wind observations, we present an accurate prediction for the arrival time and in situ parameters of corotating interaction regions (CIRs) when the Earth and Mars have large longitudinal separations. Since CIRs were detected earlier at Earth than at Mars during the period examined, we employ Earth-based CIR detections for predicting CIR observations at Mars. The arrival time is calculated by the Parker spiral model under the assumption of steady corotation of the Sun and coronal holes, while the in situ parameters are derived from Wind data through radial dependent scaling laws. The CIR prediction results are compared to the actual observations obtained from the MOMAG and Mars Ion and Neutral Particle Analyzer instruments onboard Tianwen-1, as well as the Magnetometer and Solar Wind Ion Analyzer instruments onboard MAVEN. The predicted arrival time is close to the observed values with relative errors less than 10%, and the expected in situ data show a good consistency with the Martian measurements. The comparison results indicate that the prediction method has good performance and will be helpful for comparative analysis with Tianwen-1 observations at Mars in the future.

Unified Astronomy Thesaurus concepts: Space weather (2037); Heliosphere (711)

1. Introduction

Stream interaction regions (SIRs) are formed by the interactions between the fast solar wind streams originating from coronal holes and slow solar wind streams arising in the streamer belt (Gosling & Pizzo 1999). Since the coronal holes tend to be long-lived and often persist for many months (Richardson 2018), SIRs tend to sweep past an observer at regular intervals of approximately the solar rotation period (ranging from 25 to 29 days; Jian et al. 2006). SIRs that recur on two or more solar rotations can also be referred to as corotating interaction regions (CIRs; e.g., Jian et al. 2006; Richardson 2018; Chi et al. 2022). It is essential to highlight that throughout this article, the term "CIR" is consistently employed to denote the interaction between rapid and slow solar wind, under the assumption that all events are stable and in ideal corotation (Chi et al. 2022), regardless of whether they recur more than one solar rotation.

Once CIRs sweep over the Earth, they can cause a sequence of effects, such as moderate and minor recurrent geomagnetic storms (Gosling & Pizzo 1999; Jian et al. 2006; Chi et al. 2018; Richardson 2018; Chi et al. 2022), periodic oscillations in the ionosphere (Yu et al. 2021), and variations in the Earth's neutral density in the thermosphere (Zhang et al. 2021). In rare cases, CIRs can also cause intense geomagnetic storms (Chi et al. 2018). Unlike the Earth, Mars lacks global intrinsic magnetic fields but possesses localized crustal fields that can interact directly and indirectly with the solar wind, thereby influencing the ionosphere (Connerney et al. 2015; Halekas et al. 2017; Chi et al. 2023a). Some studies have investigated the interactions between the solar wind and the Martian plasma system. Sánchez-Cano et al. (2017) found that small solar wind structures can create larger perturbations than previously expected in the Martian plasma system during solar minimum and at aphelion. Energetic particles accelerated by shocks associated with CIRs can also cause an enhancement in ionospheric ionization (Morgan et al. 2010; Lee et al. 2017).

Due to the significant influence of CIRs on the heliospheric environment, the prediction of CIRs or analysis of the properties of high-speed streams has become a matter of great concern to the space weather community. Williams et al. (2011) studied the propagation of CIRs through the inner heliosphere using a series of spacecraft and demonstrated a method for predicting the arrival of CIRs at planetary bodies and other spacecraft from ACE observations. Allen et al. (2020) analyzed the probability of sequentially detecting SIRs/CIRs at different positions by comparing SIRs/CIRs catalogs from STEREO-A/B (Jian et al. 2019) and Wind (Jian et al. 2006; Chi et al. 2018).

Chi et al. (2022) found that 58.9% of CIRs detected by STEREO-B can be used to predict the observation of Wind on Earth by calculating the summed correlation coefficient for the magnetic field, velocity, and plasma density of CIRs between two spacecraft. These studies indicate the potential capability of solar wind monitors trailing Earth in its orbit to provide an early warning of CIRs approaching at Earth several days in advance. It is worth mentioning that the discussion in Chi et al. (2022) suggested that an observer at 150 deg in longitude (HEEQ coordinates) can still provide an advanced warning for the solar wind conditions on Earth.

In addition to the studies on the time lags of CIRs between different planetary bodies or spacecraft, several analyses have also been carried out to study the in situ parameters of CIRs. Allen et al. (2021) explored the radial evolution of the CIR by scaling the plasma and field measurements according to the interplanetary magnetic field (IMF) theoretical radial dependencies and shifting the measurements in earlier times using the Parker Solar Probe and STEREO-A observations. Venzmer & Bothmer (2018) and Geyer et al. (2021) performed statistical studies to inspect the evolution of SIRs covering distances ranging from 0.29–0.98 au and 1–1.5 au, respectively, which derived exponents for the changes in solar wind parameters. These works support the prediction of in situ parameters of CIRs between spacecraft at different heliocentric distances.

Since most prior studies have focused solely on the propagation time and radial evolution of CIRs, which have often been based on a small longitudinal difference, this work intends to investigate whether the arrival time and in situ parameters of CIRs can be simultaneously predicted over large longitudinal and heliocentric distance differences. This assessment will provide ample early warning for CIRs and lead to a more comprehensive understanding of CIRs' propagation characteristics. Chi et al. (2023a) presented an SIR list based on in situ observations from Tianwen-1 (Wan et al. 2020) at Mars between 2021 November and 2021 December, when the longitudinal difference between Earth and Mars was about 160 deg. Using the SIR list, we find two Earth–Mars correlated CIRs by checking the time lags and comparing the Wind observation. Then, the prediction for arrival time and in situ parameters of CIRs with large longitudinal separation is performed. To compare the measurements between the two planets, in situ observations from Wind, Mars Atmosphere and Volatile EvolutioN (MAVEN; Jakosky et al. 2015), and Tianwen-1 are used in this study. The layout of the paper is as follows. Section 2 describes the instruments and data we use in this work. A detailed description of the events selection and prediction methods is presented in Section 3, as well as the calculation results and analysis. The conclusions and discussions of this work are given in Section 4.

2. Instruments and Data

In this study, we adopt data from the Wind (Acuna et al. 1995), which was launched on 1994 November 1 and has been stationed at L1 since 2004. One-minute resolution bulk solar wind plasma data from the Solar Wind Experiment (Ogilvie et al. 1995) and magnetic field measurements from the Magnetic Field Instrument (Lepping et al. 1995) are used to calculate the CIRs arrival time and in situ parameters on Mars.

The solar wind parameters near Mars have been continuously monitored by MAVEN since 2014 and by Tianwen-1 since 2021 November (Chi et al. 2023a; Wang et al. 2023). The Tianwen-1 spacecraft is China's first Mars exploration mission, launched on 2020 July 23, with a primary mission target of studying environmental characteristics around Mars. The Mars Orbiter Magnetometer (MOMAG; Liu et al. 2020) onboard Tianwen-1 monitors the magnetic fields around Mars to learn more about its space environment and how it interacts with the solar wind. The Mars Ion and Neutral Particle Analyzer (MINPA; Kong et al. 2020) on board Tianwen-1 is designed to detect the ions and energetic neutral atoms in the Martian environment. Since 2021 November, MOMAG and MINPA have been continuously measuring local magnetic field conditions and detecting the particles around Mars, respectively (Wang et al. 2023). The reliability of MOMAG has been verified by Zou et al. (2023), and the analysis of the background signal in MINPA also suggested that the solar wind velocity data from MINPA have good reliability (Wang et al. 2024). The MAVEN spacecraft was launched on 2013 November 18 and has been investigating the interactions of the Sun and solar wind with the Martian magnetosphere and upper atmosphere for more than 9 yr. The Magnetometer (MAG; Connerney et al. 2015) and the Solar Wind Ion Analyzer (SWIA; Halekas et al. 2015) on board MAVEN measure the intensity and direction of the magnetic field, density, temperature, bulk flow velocities, and dynamic pressure around Mars.

Since the orbits of Tianwen-1 and MAVEN are different, the observations from MAVEN are complementary to those measured from Tianwen-1 (Chi et al. 2023a). Hence, we use the combination of solar wind measurements from Tianwen-1 and MAVEN to evaluate the prediction results derived from Wind. The IMF vector data from Tianwen-1/MOMAG and MAVEN/MAG, and the solar wind plasma data from Tianwen-1/MINPA and MAVEN/SWIA are used in this study. Note that we remove the data from the period when the MAVEN and Tianwen-1 spacecraft were not exposed to background solar wind. The selection criteria for undisturbed solar wind periods are based on the descriptions in Chi et al. (2023a) and Wang et al. (2023). The velocity data from Tianwen-1/MINPA without solar wind signals in the energy spectrum (Wang et al. 2024) are also removed.

All the data used in this paper are shown in the radial–tangential–normal (RTN) coordinate system, with the x-axis pointing from the Sun center through the spacecraft (radial), the z-axis pointing along the projection of the solar north pole (normal), and the y-axis completing the right-handed coordinate system. In addition, all data have been processed using a 10 minute averaging method.

CIRs are characterized by in situ observations according to the criteria of a distinct increase in the solar wind velocity profile, a significantly enhanced magnetic field intensity, a first increase and subsequently a decrease in proton density, an increase in proton temperature, and a maximum of total pressure at the stream interface (Jian et al. 2006, 2019; Chi et al. 2018). At one au, the average duration of one SIR is about 36.7 ± 0.9 hr, the speed difference (ΔV) is 230 ± 5 km s^{-1}, and the mean maximum magnetic field intensity is 15.5 ± 0.3 nT (Jian et al. 2006). At Mars, SIRs have an average length of 37.0 ± 1.5 hr, ΔV is 178 ± 8 km s^{-1}, and the mean maximum magnetic field intensity is 11 ± 1 nT (Huang et al. 2019).

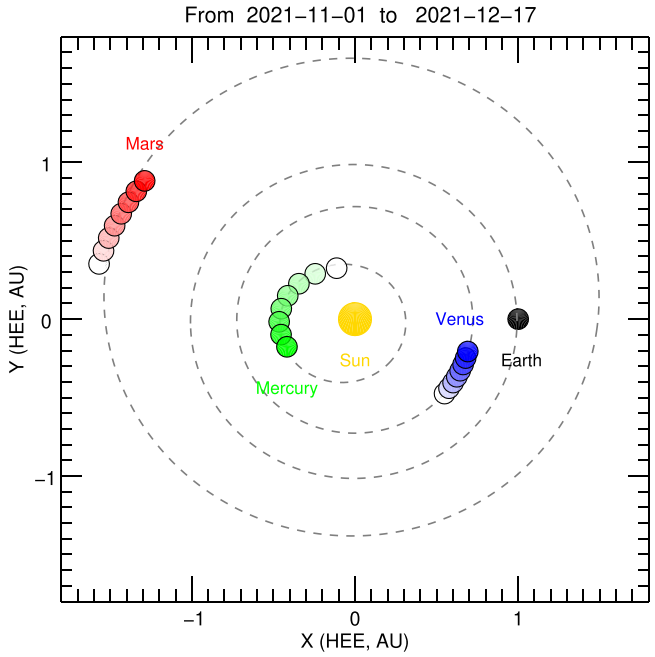

Figure 1. Positions of Mars, Mercury, Sun, Venus, and Earth in HEE coordinates from 2021 November 1 to 2021 December 17. The red dots, green dots, gold dot, blue dots, and black dot present the positions of Mars, Mercury, Sun, Venus, and Earth, respectively. The orbital track from light to dark indicates the time from earlier to later. The gray dashed curves show the orbits of the planets.

3. Observations and Analysis

3.1. Event Selection

Chi et al. (2023a) identified three SIRs at Mars observed by Tianwen-1 and found that the first (beginning at 2021-11-18T13:00; SIR-1) and third (beginning at 2021-12-16T06:00; SIR-3) SIRs have similar increasing solar wind velocity trends, magnetic field intensities, and 27.7 days gaps in arrival time, which indicate that these two fast solar wind streams are from the same coronal hole and are observed in two adjacent solar rotations. In other words, SIR-1 and SIR-3 are two CIR events (CIR-1M and CIR-2M, respectively; M represents Mars). Based on this finding, we searched for measurements from the Wind spacecraft between the beginning of CIR-1M and CIR-2M to determine whether the CIRs could be observed near Earth since most CIRs are well formed at 1 au (Huang et al. 2019).

Figure 1 shows the position of Mars, Mercury, Sun, Venus, and Earth in heliocentric Earth ecliptic (HEE) coordinates from 2021 November 1 to 2021 December 17. The orbital track from light to dark indicates the time from earlier to later. Between 2021-11-18T13:00 and 2021-12-16T06:00, the Wind observed several CIR events. Considering that the angle between Mars and Earth during this period is about 140–160 deg, the arrival time of the CIR at Earth should be roughly 15 days earlier than that at Mars (Lee et al. 2017). Therefore, we could identify the only event among these CIRs that is considered to correspond to CIR-2M, i.e., CIR-2E (E represents Earth), which has a velocity profile and magnetic field variation trend similar to those of CIR-2M and begins at 2021-11-30T13:42. CIR-2E has a duration of about 19 hr, while the duration of CIR-2M is 22 hr. These CIRs have much shorter durations than the typical duration of CIRs both on Earth and on Mars (Jian et al. 2006; Huang et al. 2019). The small difference in the duration of CIR-2E and CIR-2M indicates that CIRs did not expand significantly from Earth to Mars, which is consistent with previous findings (Huang et al. 2019; Geyer et al. 2021).

Since the corresponding observation of CIR-2M was obtained by Wind, it can be easily inferred that the counterpart of CIR-1M at Earth can also be found, i.e., CIR-1E. The arrival time of CIR-1E should satisfy two criteria: (i) approximately one solar rotation earlier than CIR-2E; (ii) approximately 15 days earlier than CIR-1M. Using these criteria, we found the observations of CIR-1E successfully, which is about 29.0 days earlier than those of CIR-2E and about 16.9 days earlier than those of CIR-1M. The duration of CIR-1E is the same as CIR-1M, which is about 24 hr. The beginning and end of these two CIRs at Earth, the time of Stream Interface (SI) and the mean values of the total magnetic field intensity (B), the southern component of the magnetic field (B_s), the solar wind velocity ($v_{\rm sw}$), the proton temperature (T_p), the plasma density (N_p), and the dynamic pressure ($P_{\rm dp}$) in the CIRs are listed in Table 1. The mean values of these parameters of CIR-1E are close to those of CIR-2E.

To further confirm whether CIR-1E and CIR-2E are correlated CIRs, in addition to confirming their time lags, we compared their in situ parameters from Wind, as shown in Figure 2. CIR-2E has been moved forward by 29.0 days to align its beginning with that of CIR-1E, and the measurements of these two CIRs have not been stretched or compressed since their durations are similar. Figures 2(a)–(e) show the total magnetic field intensity ($|B|$), N component of the magnetic field in the RTN coordinate system (B_n) from Wind, solar wind speed, plasma density, and proton temperature. The black asterisk indicates CIR-1E, and the red asterisk indicates the time-shifted CIR-2E. As the arrows show, the vertical orange solid lines represent the beginning and end of CIR-1E, while the vertical dashed lines with the same color represent the beginning and end of CIR-2E. Note that the beginning of these two CIRs are overlapped. The vertical blue solid line represents the SI of CIR-1E, which is close to that of CIR-2E with a vertical blue dashed line. The comparison in Figure 2 shows that the magnetic fields, solar wind velocities, plasma densities, and proton temperatures of CIR-1E and CIR-2E not only exhibit very consistent trends but also exhibit little difference in value, while the high-speed stream in CIR-1E has a greater velocity than that in CIR-2E, and the maximum proton temperature of CIR-2E is relatively larger.

Since the in situ parameters of CIR-1E and CIR-2E are close to each other, and the time lags between them are approximately one solar rotation, it is credible to derive that they are correlated CIRs. In total, a comprehensive scenario of these CIRs during the period of study can be described as follows: the high-speed stream from the coronal hole interacted with the slow solar wind and formed the CIR, which was observed by Wind (CIR-1E) near Earth; about 16.9 days later, the CIR also swept the spacecraft (Tianwen-1 and MAVEN) near Mars (CIR-1M); one solar rotation after the CIR-1E, the CIR was observed by Wind once again (CIR-2E), and was sequentially detected at Mars (CIR-2M). These two Earth–Mars correlated CIRs (CIR-1 and CIR-2) will be used to perform the prediction for CIR at Mars based on observation from Earth in this work.

3.2. Prediction Method

It is assumed that a stable CIR structure has formed overall from Earth orbit to Mars orbit before the period of study, and

Table 1
Beginning and End Times of CIRs Detected by the Wind Spacecraft on Earth

Symbol	Begin Time of the CIR	End Time of the CIR	Time of Stream Interface	Mean Values in the CIR					
				B	B_s	v_{sw}	T_p	N_p	P_{dp}
	(UT)	(UT)	(UT)	(nT)	(nT)	(km s^{-1})	(10^5 K)	(cm^{-3})	(nPa)
CIR-1E	2021-11-01T15:00	2021-11-02T15:20	2021-11-01T21:00	6.85	−1.34	497.5	1.66	9.94	1.59
CIR-2E	2021-11-30T13:42	2021-12-01T08:34	2021-11-30T19:51	8.05	0.92	445.61	2.08	12.01	1.74

this structure ideally corotates with the Sun. In addition, there are no other structures, such as coronal mass ejections (CMEs), that interact with the CIR. Under these assumptions, the front edge of the CIR is similar to the Parker spiral (Richardson 2018). Spacecraft at different positions on the same Parker spiral can observe the CIR at the same time. According to the descriptions in Hundhausen (1972), the Parker spiral equation in a spherical coordinate system (R, ϕ, θ) rotating with the Sun can be expressed as

$$R - R_0 = \frac{-v_{sw}}{\Omega \sin\theta}(\phi - \phi_0), \quad (1)$$

where ϕ_0 represents the initial position at a reference heliocentric distance R_0, v_{sw} represents the radial solar wind velocity, which is thought to be a constant (Hundhausen 1972; Richardson 2018), and Ω represents the solar rotation angular velocity. From Equation (1), it can be derived that an observer at Mars orbit observing one CIR simultaneously as the Earth should have longitude lags behind the Earth due to the curvature of the Parker spiral. The value of the longitude lags (ϕ_p) is

$$\phi_p = \phi_{E0} - \phi_{M0} = \frac{\omega}{v_{sw}}(R_{M0} - R_{E0}). \quad (2)$$

The symbols in Equation (2) with subscript 0 represent parameters at initial time t_0, which is the arrival time of the CIR at Earth, $\omega = \Omega\, sin\theta$ is the solar rotation speed at the latitude (θ) of coronal hole, subscripts E and M represent the parameters at the Earth orbit and Mars orbit, respectively. In addition, considering that the orbital radii of Mars and Earth are relatively stable, we assume that $\Delta R = R_{M0} - R_{E0}$ is a constant value during the period we investigate. Hence, the time lags of the CIR between Earth and Mars consist of two parts, one is from the difference in longitude ($\Delta\phi$), and the other is from ϕ_p. The arrival time of the CIR at Mars is

$$t_{cal} = t_0 + \frac{\Delta\phi + \phi_p}{\omega - \omega_r} = t_0 + \frac{\Delta\phi}{\omega - \omega_r} + \frac{\omega}{\omega - \omega_r}\frac{\Delta R}{v_{sw}}, \quad (3)$$

where ω_r represents the relative motion of the Mars to the Earth (Allen et al. 2020). Equation (3) is used to predict the arrival time of CIRs at Mars based on parameters from Earth in this work.

It is worth noting that Equation (3) is not limited to calculating the time of CIRs from Earth to Mars, and it can also be used between any two planetary bodies or spacecraft. Moreover, when the relative velocity is small, i.e., ω_r can be ignored and Equation (3) can be simplified as

$$t_{cal} = t_0 + \frac{\Delta\phi}{\omega} + \frac{\Delta R}{v_{sw}}, \quad (4)$$

which has the same form as the calculation method of the CIR propagation times in previous work (e.g., Richardson et al. 1998; Opitz et al. 2009; Williams et al. 2011; Richardson 2018; Jian et al. 2019; Geyer et al. 2021; Chi et al. 2022).

In this study, CIRs are assumed to be large-scale structures with stable distributions in the interplanetary space within Mars orbit. The distributions of the magnetic field and plasma parameters of CIRs are considered to be radially dependent (Kivelson & Russell 1995; Allen et al. 2021). The approximate scaling laws can be expressed as follows: $B_r \propto r^{-2}$, $B_t \propto r^{-1}$, $n \propto r^{-2}$, $T \propto r^{-4/3}$, where B_r and B_t denote the radial and tangential components of the IMF in RTN coordinates. These rules are proven by Allen et al. (2021) to be well applicable to the radial evolution analysis of the CIRs. The radial solar wind velocity is an important parameter to be used in calculating the arrival time of CIRs and is considered to be a constant in this study (e.g., Williams et al. 2011). The normal magnetic field component (B_n) in the quiet solar wind is approximately zero, while B_n is nonzero in the interaction region. Since the Parker solar wind model (e.g., Hundhausen 1972; Kivelson & Russell 1995) does not give the radial distribution law of B_n, an approximate method that $B_n \propto r^{-1}$ is used in this work.

3.3. Calculation and Analysis

The arrival time or the front edge observation time is the primary concern for CIR prediction, which can be calculated using a model based on Equation (3). The initial parameters for calculation are listed in the first column in Table 2, where t_0 is the front of CIRs at Earth by Wind, i.e., the initial time; $\Delta\phi$ represents the longitudinal difference between Mars and Earth at t_0; ω represents the angular velocity of CIRs corotating with the Sun; ω_r represents the angular velocity of Mars relative to the Earth; ΔR represents the heliocentric distance between Mars and Earth at beginning; v_{sw} is the radial solar wind velocity in the CIR front at Earth, i.e., the slow solar wind before interaction region. It is worth noting that although the equatorial rotation speed of the Sun is about 14.7 deg day^{-1} (24.5 days for one solar rotation; Allen et al. 2020), the CIRs' rotation period is considered to be different (e.g., 27.13 days for one solar rotation; Owens et al. 2013; Chi et al. 2022). Moreover, solar rotation is known to have a latitudinal dependence (Allen et al. 2020), and the time window of one solar rotation can range from 25 to 29 days (Jian et al. 2006). In this study, the time lag between the beginnings of CIR-1E and CIR-2E is about 29 days, which is used to calculate the solar rotation speed for a more practical CIR prediction, i.e., $\omega = 12.41$ deg day^{-1}.

The calculation results of the prediction for CIRs arriving at Mars are listed in Table 2. The second column shows the theoretical time lags between the CIR arrival times at Earth and Mars, and the third column shows the theoretical arrival times

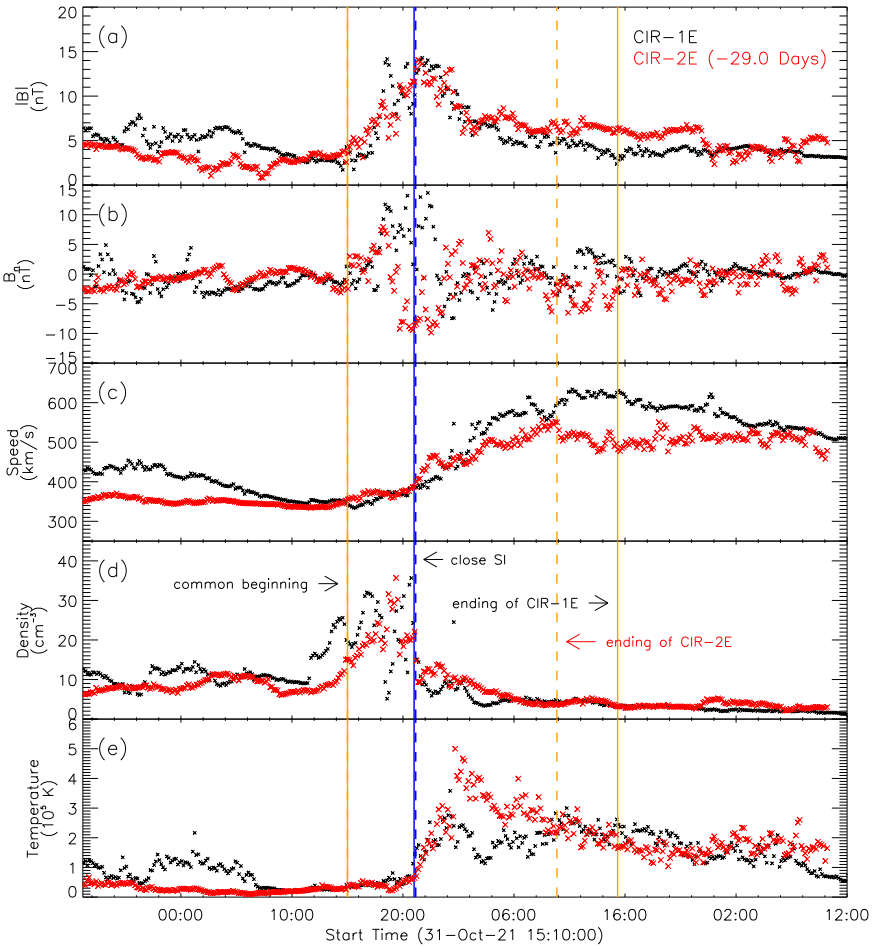

Figure 2. Comparison of CIR-1E and time-shifted CIR-2E from Wind. As denoted by arrows in panel (d), the vertical orange solid lines represent the beginning and end of CIR-1E, and the vertical dashed lines with the same color represent the beginning and end of CIR-2E. The vertical blue solid line represents the SI of CIR-1E, which is close to the SI of CIR-2E with the vertical blue dashed line.

of the CIRs at Mars. The actual observations from Tianwen-1 of these CIRs are listed in the fourth column (Chi et al. 2023a). The last column shows the prediction deviation from the actual observation (theoretical value minus the observation).

The prediction deviation shows that the predicted arrival times for these two CIRs are earlier than the actual observation, while the deviations are less than 30 hr and the relative errors are 6.08% and 6.83%, respectively. These results are comparable with the conclusions in Williams et al. (2011), which suggest that all CIRs they studied can be found within 1.5 days of the calculation results.

As mentioned in Section 3.2, the approximate scaling laws are applied to derive the in situ parameters at Mars orbit from L1 point observation by Wind. Figure 3 shows the comparison between in situ measurements at Mars and the value predicted from the Earth for CIR-1. The red asterisks are Tianwen-1 observations, black asterisks represent MAVEN observations, and blue diamonds represent the scaled and time-shifted Wind observations, which are also indicated at the top right of Figure 3. Note that the shift time (+16.92 days) for Wind is determined by the actual time lags between the fronts of CIR-1E and CIR-1M, and the duration of CIR-1E is not scaled since it is similar to the duration of CIR-1M. Comparison in Figure 4 is also conducted in the same way. In Figure 3, panels (a)–(i) show the total magnetic field intensity ($|B|$), three components of the magnetic field in the RTN coordinate system (B_r, B_t, and B_n), the solar wind speed (V_{sw}), plasma density, the proton temperature, the total pressure, and the plasma beta (β_p). The gray-colored band indicates the interval of the CIR-1M (from 2021-11-18T13:00 to 2021-11-19T13:00) inferred from the Tianwen-1 data (Chi et al. 2023a), while the yellow vertical solid line shows the SI of CIR-1M at 18:30 on 2021 November 18. The separation angle and separation distance at the start time (2021-11-17T15:00:00) of Figure 3 between Mars and Earth are 158.50 deg and 0.60 au, respectively. The change in the separation angle is about 8.49 deg from 2021 November 1 to 2021 November 17, which shows that it is necessary to take the relative angular velocity (ω_r) into account in the calculation, and the almost constant separation distance also shows that it is reasonable to assume that ΔR is constant.

As shown in Figure 3, the scaled Wind data are comparable to the data obtained from the combination of Tianwen-1 and MAVEN (the Martian observation). The maximum of the total magnetic field from the scaled Wind data is close to the Martian observation, while the former has steeper increasing and decreasing trends. The three components of the magnetic field are very consistent between the predicted and observed values. However, the velocity difference between the fast and slow solar winds is not as large as expected, i.e., the Martian solar wind profile is flatter. The density profile of the scaled Wind matches well in the CIR region with that of the Martian observation, while some enhancement occurs before the CIR at

Table 2
Comparison of CIRs Prediction Results with Observations

Initial Parameters	Theoretical Time Lag (days)	Theoretical Arrival Time at Mars (UT)	Observation Time by Tianwen-1 [a] (UT)	Prediction Deviation (hr)
t_0: 2021-11-01T15:00 $\Delta\phi$: 166.99 deg ω: 12.41 deg day^{-1} ω_r: −0.53 deg day^{-1} ΔR: 0.61 au v_{sw}: 341.53 km s^{-1}	15.89	2021-11-17T12:18	2021-11-18T13:00	−24.69
t_0: 2021-11-30T13:42 $\Delta\phi$: 151.68 deg ω: 12.41 deg day^{-1} ω_r: −0.52 deg day^{-1} ΔR: 0.59 au v_{sw}: 339.44 km s^{-1}	14.61	2021-12-15T04:18	2021-12-16T06:00	−25.69

Note.
[a] From Chi et al. (2023a).

Mar. The total pressure calculated by the magnetic field strength, density, and temperature also show similar maxima but sharper profiles than Martian observations. As suggested in Geyer et al. (2021), the discrepancies in $|B|$, V_{sw}, and the total pressure profile between the predicted and actual data may be due to wave crest broadening with respect to the expansion of the steam close to the SI. The predicted temperature is lower than the observed value, especially in the high-temperature region, which indicates that the proton temperature decays at a slower rate (e.g., $T \propto r^{-0.69}$ in Marsch & Richter 1984) with increasing heliocentric distance than expected if the solar wind was adiabatic expansion ($T \propto r^{-4/3}$).

Figure 4 shows a comparison between the scaled and time-shifted Wind and Martian observations of CIR-2. The plot setup is the same as that in Figure 3. The gray-colored band indicates the interval of the CIR-2M (from 2021-12-16T06:00 to 2021-12-17T04:00; Chi et al. 2023a), while the yellow vertical solid line shows the SI of CIR-2M at 19:40 on December 16. For CIR-2, the profiles of the total magnetic field, three components of the magnetic field, and the solar wind velocity for the scaled Wind are well consistent with the actual observations. The plasma density, proton temperature, and total pressure for the predicted values all have the same trends as those of the Martian observation, although the overall values are lower.

As shown in Figures 3 and 4, the consistency of the magnetic field and plasma parameters between the time-shifted scaled Wind and the combination of the Tianwen-1 and MAVEN indicates that the approximate scaling laws mentioned in Section 3.2 can be used to predict the in situ parameters at Mars based on the observations from the Earth. Moreover, this finding provides strong evidence for the correlation of the CIRs observed on both the Earth and Mars.

4. Conclusions and Discussions

4.1. Conclusions

Based on the SIR list in Chi et al. (2023a), which used the Tianwen-1/MOMAG data between 2021 November and 2021 December, we present the corresponding two CIRs at Earth that are observed in two adjacent solar rotations by checking the arrival time of the CIRs both at Earth and at Mars. These two events are confirmed once again to be the same CIR by comparing their in situ measurements from the Wind. During the period of study, the separation longitudinal angle between the Earth and Mars decreases with time from about 167 deg to about 142 deg, while their difference in heliocentric distance fluctuates around 0.6 au. These two Earth–Mars correlated CIRs provide us with an opportunity to test CIR prediction between planetary bodies with large longitudinal differences and different heliocentric distances. In this work, prediction for arrival time and in situ parameters of CIRs at Mars are performed by the observations at Earth, and the results are compared between the predicted and actual values using Tianwen-1, MAVEN, and Wind data. The conclusions are summarized as follows:

1. The arrival time of CIRs at Mars is predicted by assuming that the front of the CIR is Parker-spiral-like and corotates steadily with the Sun. The relative angular speed of Mars (about −0.5 deg day^{-1}) with respect to Earth is also taken into account. As shown by the calculation results, the time lags are about 15.89 days for CIR-1 observing successively by spacecraft at Earth and Mars with a longitudinal difference of about 166.99 deg, a heliocentric distance of about 0.61 au, and a radial solar wind velocity of about 341.53 km s^{-1}. For CIR-2, the time lags are about 14.61 days, while the longitudinal difference is about 151.68 deg, the heliocentric distance is about 0.59 au, and the radial solar wind velocity is about 339.44 km s^{-1}. The predicted arrival times of two CIRs are about 24.69 and 25.69 hr earlier than the actual observations, respectively, while the relative errors are about 6.08% and 6.83%, which are comparable with previous studies (Williams et al. 2011; Jian et al. 2019). Note that a 29 day Solar rotation is used according to the time lags between the beginnings of two CIRs at Earth for a more practical and accurate prediction in this study.
2. The magnetic field and plasma parameters of the CIRs at Earth are scaled and time-shifted to predict the observations at Mars according to the approximate scaling laws (Kivelson & Russell 1995; Allen et al. 2021), i.e., $B_r \propto r^{-2}$, $B_t \propto r^{-1}$, $B_n \propto r^{-1}$, $n \propto r^{-2}$, $T \propto r^{-4/3}$. Comparisons between the predicted and actual values are carried out to check the accuracy of this method. The results show that the predicted values are generally in

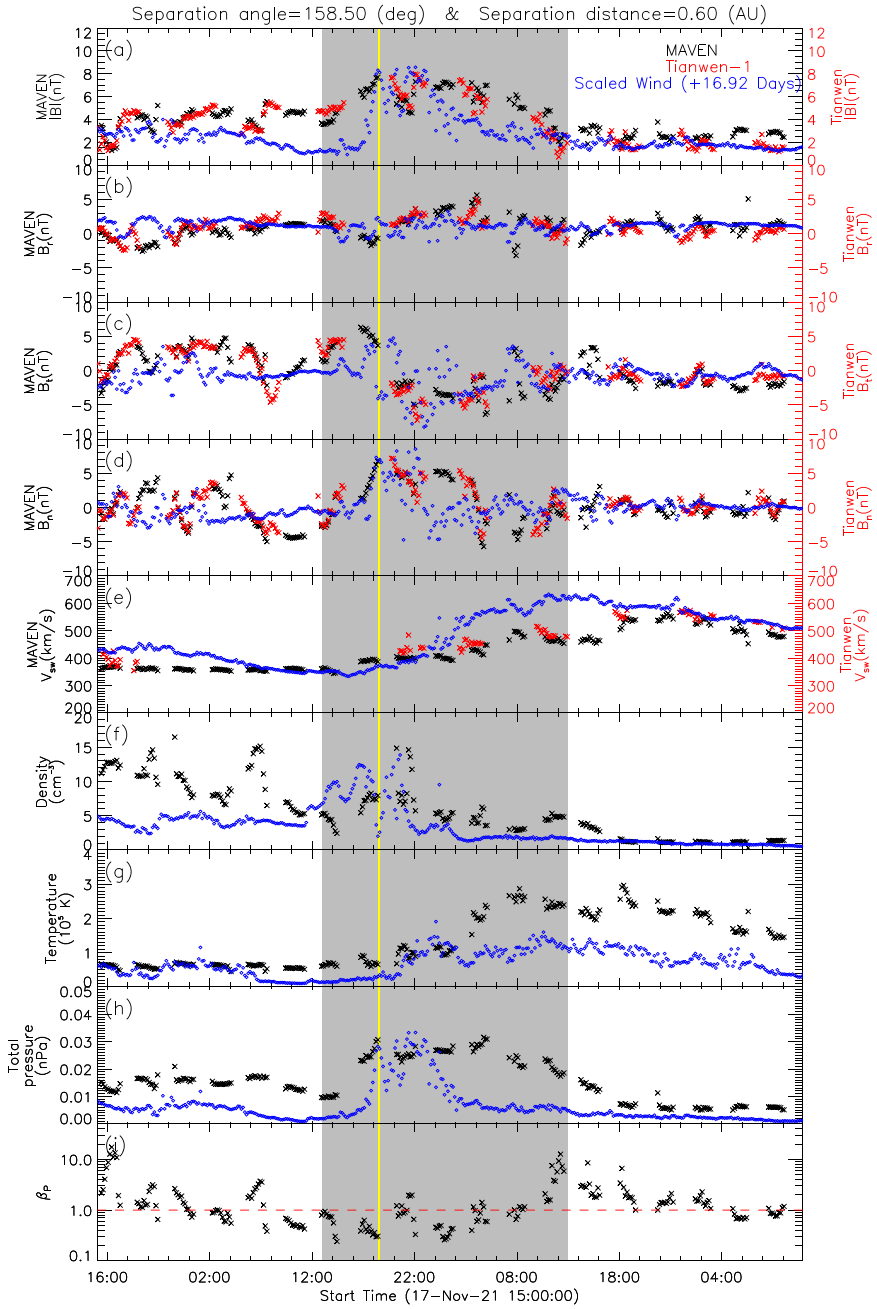

Figure 3. Comparison between the in situ measurement at Mars and the predicted value from the Earth for CIR-1. The black asterisks represent MAVEN observations, the red asterisks are Tianwen-1 observations, and the blue diamonds represent the scaled and time-shifted Wind observations. The gray-colored band indicates the interval of the CIR-1M (from 2021-11-18T13:00 to 2021-11-19T13:00) inferred from the Tianwen-1 data (Chi et al. 2023a), while the yellow vertical solid line shows the SI of CIR-1M at 18:30 on 2021 November 18. The separation angle and separation distance between Mars and Earth at the start time of this figure are presented in the title. The shifted time is about 16.92 days.

good agreement with the observed values, although having some discrepancies. Similar comparisons for investigating the radial evolution of CIRs have also been done by Venzmer & Bothmer (2018) and Geyer et al. (2021), as discussed later.

This is the first study to predict the arrival time and in situ parameters of the CIRs with longitudinal differences larger than 150 deg and radial differences of about 0.6 au. The good prediction results show the feasibility of our method, which is conducive to achieving a more comprehensive study of Mars since there are fewer instruments available near Mars than near Earth, and spacecraft such as Tianwen-1 often lose reliable solar wind observations as they enter the Martian magnetosphere (Chi et al. 2023a; Zou et al. 2023). Moreover, our method can also be applied to the analysis between any two planetary bodies or spacecraft. For example, the arrival time of the CIRs at BepiColombo (Benkhoff et al. 2021) during its cruise phase can also be calculated based on the beginning of CIR at Earth. For CIR-1, the results predicted by our model show that the arrival time is 2021-11-08T04:30 at BepiColombo. During this time, the heliocentric distance of BepiColombo was about 0.5 au, while its angular separation from Earth was about 112 deg, positioning it midway between Earth and Mars. By checking the data from the magnetometer

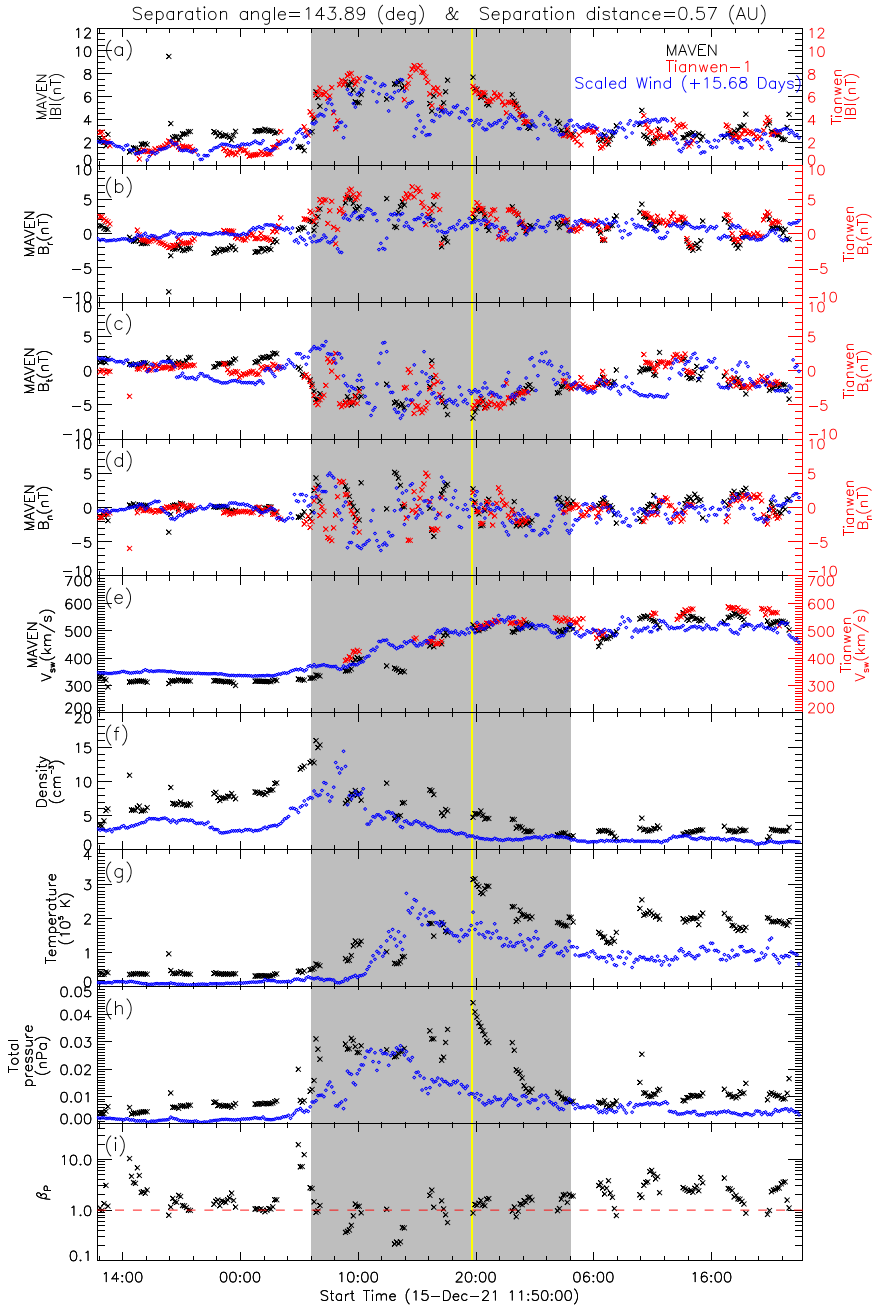

Figure 4. Comparison between the in situ measurement at Mars and the predicted value from the Earth for CIR-2. The plot setup is the same as that in Figure 3. The gray-colored band indicates the interval of the CIR-2M (from 2021-12-16T06:00 to 2021-12-17T04:00; Chi et al. 2023a), while the yellow vertical solid line shows the SI of CIR-2M at 19:40 on December 16. The shifted time is about 15.68 days.

instrument on board the Mercury Planetary Orbiter (MPO-MAG; Heyner et al. 2021) of BepiColombo, we find that the actual observation time of CIR-1 at BepiColombo is approximately 2021-11-07T14:00 and the deviation of the arrival times between the predicted value and observed value is 14.5 hr. Due to the lack of plasma data, further confirmation of the correlation between the observations at BepiColombo and Wind could not be obtained. Nevertheless, our method demonstrates the ability to identify CIRs within a large data set.

4.2. Discussions

It is not too difficult to spot that the expected arrival of CIR-1 at BepiColombo is later than the actual observation, while the predicted results of both CIR-1 and CIR-2 at Mars are earlier. The possible reason for the discrepancy may be the simplification of the Parker spiral model used in our method. Since the CIR results from the interaction between the fast and slow solar winds, the interaction region becomes increasingly larger as the heliocentric distance increases (Richardson 2018), which indicates greater compression with increasing heliocentric distance. The deformation of the IMF structure outside of the Parker spiral causes the deviation of the prediction. Moreover, the prediction results that the arrival time of CIR-1 is earlier than expected at BepiColombo but later than expected at Mars also indicate that the rotation of the CIRs is not constant (Allen et al. 2020) or the coronal holes have developed and evolved (Richardson 2018; Chi et al. 2022), which is different from the

Table 3
Comparison of RMS Error Among Different Scaling Laws

No.	Parameters (Unit)	RMS Error (Scaling Laws)		
		Our Methods	Venzmer & Bothmer (2018)	Geyer et al. (2021)
1	$\|B\|$ (nT)	2.16	2.18 ($r^{-1.55}$)	2.24 ($r^{-1.63}$)
	B_r (nT)	1.81 (r^{-2})	…	…
	B_t (nT)	3.01 (r^{-1})	…	…
	B_n (nT)	3.14 (r^{-1})	…	…
	V_{sw} (km s^{-1})	75.28 (r^{0})	84.64 ($r^{+0.05}$)	67.87 ($r^{-0.53}$)
	Density (cm^{-3})	4.72 (r^{-2})	4.72 ($r^{-2.01}$)	4.71 ($r^{-1.99}$)
	Temperature (10^5 K)	0.87 ($r^{-\frac{4}{3}}$)	0.72 ($r^{-0.79}$)	1.02 ($r^{-1.92}$)
	Total Pressure (nPa)	1.18×10^{-2}	1.16×10^{-2}	1.29×10^{-2}
2	$\|B\|$ (nT)	1.41	1.56	1.62
	B_x (nT)	2.15	…	…
	B_y (nT)	2.39	…	…
	B_z (nT)	2.47	…	…
	V_{sw} (km s^{-1})	34.37	37.53	95.51
	Density (cm^{-3})	3.88	3.90	3.87
	Temperature (10^5 K)	0.76	0.61	0.92
	Total Pressure (nPa)	1.08×10^{-2}	1.10×10^{-2}	1.23×10^{-2}

assumption we have made (see Section 3.2) and may result in uncertainty in the rotational speed of the structure Allen et al. (2020). Hence, multiple longitudinally spaced spacecraft such as twin STEREO before 2015, can help determine the variable rotational speed of the SIR/CIR (Allen et al. 2020). The solar wind monitor located at 30 deg and 150 deg longitude ahead of the Sun–Earth line (Solar Ring) has been proposed by Wang et al. (2020), which will hopefully improve the capabilities for CIR prediction.

Previous studies have identified CME events that occurred during the study period (e.g., Chi et al. 2023a, 2023b; Yu et al. 2023). These CMEs may have cleared some of the ambient solar wind plasma (Chi et al. 2020), leading to a rarefied and disturbed solar wind; consequently, the prediction for the in situ parameters of CIRs is affected. However, the prediction for the arrival time of CIRs at Mars is unaffected because these CMEs did not interact with the CIRs. In addition to the impact of CMEs, the inconsistencies observed when comparing the scaled and time-shifted Wind and Martian measurements could be due to the fact that the approximate scaling laws outlined in Section 3.2 are not entirely applicable to all parameters of the CIRs studied, particularly the plasma density and proton temperature. These rules are derived from the general solar wind magnetic field and plasma parameters, and their validity could be limited when applied to CIRs. Venzmer & Bothmer (2018) derived exponents for the decrease or increase in solar wind parameters from 0.3 to 1 au based on data from Helios 1+2 and OMNI, while Geyer et al. (2021) focused on the distance range of 1–1.5 au by comparing SIRs at Earth and Mars. To compare the capabilities of the scaling laws in Venzmer & Bothmer (2018) and Geyer et al. (2021) with our methods, the rms errors are calculated for two CIRs, as listed in Table 3.

In Table 3, the parameters have the same meanings as in Figures 3 and 4. The rms error is calculated by $\sqrt{\frac{\Sigma(\text{Martian Observation} - \text{Scaled Value})^2}{N}}$, where N represents the number of data in one parameter. As shown by the comparison, the scaling laws in the three methods for $|\boldsymbol{B}|$, *Density* have similar performances, while the law for *Temperature* in Venzmer & Bothmer (2018) has better results. The exponent for V_{sw} in Geyer et al. (2021) achieves the smallest rms error in CIR-1, but has the largest rms error in CIR-2. The total pressure, the sum of thermal and magnetic pressure, is determined by $|\boldsymbol{B}|$, the density, and the temperature. Consequently, the performance of these three parameters directly impacts the rms error of the total pressure. As presented in Table 3, the rms errors of the total pressure in our methods and in Venzmer & Bothmer (2018) are comparable, while the rms error in Geyer et al. (2021) is slightly higher. In total, there is no single method among them that is perfect for all parameters of both CIRs. Moreover, it is worth noting that although Venzmer & Bothmer (2018) and Geyer et al. (2021) performed statistical analysis of the radial evolution of CIRs, their studies focused on the properties of all the CIRs that were averaged without correlating the events at different positions. Hence, a statistical study of correlated CIR events needs to be carried out to investigate a better radially dependent scaling law for CIRs in the future.

Acknowledgments

We acknowledge the use of the data from the Wind spacecraft. The Wind/MFI and Wind/SWE data are downloaded from NASA's Space Physics Data Facility (SPDF; http://spdf.gsfc.nasa.gov/). We acknowledge the Tianwen-1/MOMAG and Tianwen-1/MINPA team for providing the magnetic field and plasma data. The Tianwen-1/MOMAG and Tianwen-1/MINPA data are accessible through the Planet Exploration Program Scientific Data Release System (http://202.106.152.98:8081/marsdata/), and the MOMAG data used in this study can be downloaded from the official website of the MOMAG team (http://space.ustc.edu.cn/dreams/tw1_momag/). All MAVEN data used in this study are available through the MAVEN Science Data Center (https://lasp.colorado.edu/maven/sdc/public/). We acknowledge the BepiColombo/MPO-MAG team for providing the MPO-MAG data for investigating the CIR.

This work is supported by grants from the NSFC (42325405, 42130204, 41904151, 42188101, 42074222), the Key Research Program of the Chinese Academy of Sciences, grant No. ZDBS-SSW-TLC00103, the Strategic Priority Program of the Chinese Academy of Sciences (XDB41000000), the CNSA pre-research Project on Civil Aerospace Technologies (grant D020104), the Frontier Scientific Research Program of Deep Space Exploration-Laboratory (2022-QYKYJH-ZYTS-016), and the International Space Science Institute (ISSI) in Bern and Beijing, through ISSI/ISSI-BJ International Team project "Understanding the Mars Space Environment through Multi-Spacecraft Measurements" (ISSI Team project #23-582; ISSI-BJ Team project #58).

ORCID iDs

Zhihui Zhong https://orcid.org/0000-0002-5627-2377
Chenglong Shen https://orcid.org/0000-0002-3577-5223
Yutian Chi https://orcid.org/0000-0001-9315-4487
Zhiyi Fu https://orcid.org/0009-0005-3921-1360
Junyan Liu https://orcid.org/0009-0006-7051-0438
Beatriz Sánchez-Cano https://orcid.org/0000-0003-0277-3253
Yuming Wang https://orcid.org/0000-0002-8887-3919

References

Acuna, M. H., Ogilvie, K. W., Baker, D. N., et al. 1995, SSRv, 71, 5
Allen, R. C., Ho, G. C., Jian, L. K., et al. 2020, SpWea, 18, 11

Allen, R. C., Ho, G. C., Mason, G. M., et al. 2021, GeoRL, 48, e91376
Benkhoff, J., Murakami, G., Baumjohann, W., et al. 2021, SSRv, 217, 90
Chi, Y., Scott, C., Shen, C., et al. 2020, ApJ, 899, 143
Chi, Y., Shen, C., Luo, B., Wang, Y., & Xu, M. 2018, SpWea, 16, 1960
Chi, Y. T., Shen, C. L., Cheng, L., et al. 2023a, ApJS, 267, 3
Chi, Y. T., Shen, C. L., Liu, J. Y., et al. 2023b, ApJL, 951, L14
Chi, Y. T., Shen, C. L., Scott, C., et al. 2022, SpWea, 20, 11
Connerney, J. E. P., Espley, J. R., DiBraccio, G. A., et al. 2015, GeoRL, 42, 8819
Geyer, P., Temmer, M., Guo, J. N., & Heinemann, S. G. 2021, A&A, 649, 20
Gosling, J. T., & Pizzo, V. J. 1999, SSRv, 89, 21
Halekas, J. S., Ruhunusiri, S., Harada, Y., et al. 2017, JGRA, 122, 547
Halekas, J. S., Taylor, E. R., Dalton, G., et al. 2015, SSRv, 195, 125
Heyner, D., Auster, H. U., Fornaçon, K. H., et al. 2021, SSRv, 217, 52
Huang, H., Guo, J. P., Wang, Z. H., et al. 2019, ApJ, 879, 118
Hundhausen, A. J. 1972, Coronal Expansion and Solar Wind, Physics and Chemistry in Space (Berlin: Springer)
Jakosky, B. M., Grebowsky, J. M., Luhmann, J. G., & Brain, D. A. 2015, GeoRL, 42, 8791
Jian, L., Russell, C. T., Luhmann, J. G., & Skoug, R. M. 2006, SoPh, 239, 337
Jian, L. K., Luhmann, J. G., Russell, C. T., & Galvin, A. B. 2019, SoPh, 294, 31
Kivelson, M. G., & Russell, C. T. 1995, Introduction to Space Physics (New York: Cambridge Univ. Press)
Kong, L. G., Zhang, A. B., Tian, Z., et al. 2020, E&PP, 4, 333
Lee, C. O., Hara, T., Halekas, J. S., et al. 2017, JGRA, 122, 2768
Lepping, R. P., Acuna, M. H., Burlaga, L. F., et al. 1995, SSRv, 71, 207
Liu, K., Hao, X. J., Li, Y. R., et al. 2020, E&PP, 4, 384
Marsch, E., & Richter, A. K. 1984, JGR, 89, 6599
Morgan, D. D., Gurnett, D. A., Kirchner, D. L., et al. 2010, Icar, 206, 95
Ogilvie, K. W., Chornay, D. J., Fritzenreiter, R. J., et al. 1995, SSRv, 71, 55
Opitz, A., Karrer, R., Wurz, P., et al. 2009, SoPh, 256, 365
Owens, M. J., Challen, R., Methven, J., Henley, E., & Jackson, D. R. 2013, SpWea, 11, 225
Richardson, I. G. 2018, LRSP, 15, 1
Richardson, I. G., Mazur, J. E., & Mason, G. M. 1998, JGR, 103, 2115
Sánchez-Cano, B., Hall, B. E. S., Lester, M., et al. 2017, JGRA, 122, 6611
Venzmer, M. S., & Bothmer, V. 2018, A&A, 611, A36
Wan, W. X., Wang, C., Li, C. L., & Wei, Y. 2020, NatAs, 4, 721
Wang, Y., Ji, H., Wang, Y., et al. 2020, ScChE, 63, 1699
Wang, Y. M., Zhang, T. L., Wang, G. Q., et al. 2023, E&PP, 7, 216
Wang, Z. Y., Miao, B., Wang, Y. M., Shen, C. L., et al. 2024, arXiv:2403.13693
Williams, A. O., Edberg, N. J. T., Milan, S. E., et al. 2011, JGRA, 116, A08103
Yu, B. K., Chi, Y. T., Owens, M., et al. 2023, ApJ, 953, 105
Yu, B. K., Scott, C. J., Xue, X. H., et al. 2021, ApJ, 916, 106
Zhang, J., Temmer, M., Gopalswamy, N., et al. 2021, PEPS, 8, 56
Zou, Z. X., Wang, Y. M., Zhang, T. L., et al. 2023, ScChE, 66, 2396